Multifrequency Polarimetric SAR Image Despeckling by Iterative Nonlocal Means Based on a Space-Frequency Information Joint Covariance Matrix

Xiaoshuang Ma ⓘ, Penghai Wu ⓘ, *Member, IEEE*, and Huanfeng Shen ⓘ, *Senior Member, IEEE*

Abstract—**This paper presents an iterative nonlocal means (NLM) filtering method under the Bayesian framework to deal with the issue of multifrequency fully polarimetric synthetic aperture radar (PolSAR) image despeckling. Differing from most of the Pol-SAR filters designed for single-frequency data, the proposed NLM method is developed based on a space-frequency information joint covariance matrix, which can not only utilize multifrequency polarimetric information but also exploit the correlation between any two pixels in an image patch. Furthermore, with the aim of accelerating the filtering procedure and better retaining image details, an effective preselection step is employed. The filtering results obtained with both a simulated dataset and real multifrequency Pol-SAR datasets acquired by the AIRSAR system confirm the good performance of the proposed method in both reducing speckle and retaining details, when compared with some of the state-of-the-art despeckling algorithms.**

Index Terms—**Nonlocal means (NLM), polarimetric synthetic aperture radar (PolSAR), speckle filtering, Wishart distribution.**

I. INTRODUCTION

POLARIMETRIC synthetic aperture radar (PolSAR) systems are capable of emitting and receiving fully polarized radar waves to characterize observed targets, together with all-weather, day-and-night imaging capabilities, resulting in their wide use. However, due to the coherent nature of SAR systems, PolSAR data are inherently affected by speckle noise,

X. Ma is with the Department of Resources and Environmental Engineering, Anhui University, Hefei 230601, China (e-mail: mxs.88@whu.edu.cn).

P. Wu is with the Department of Resources and Environmental Engineering, Anhui University, Hefei 230601 China, and also with the Institute of Physical Science and Information Technology, Anhui University, Hefei 230601, China (e-mail: wuph@ahu.edu.cn).

H. Shen is with the Department of Resource and Environmental Sciences, Wuhan University, Wuhan 430079, China (e-mail: shenhf@whu.edu.cn).

which complicates the interpretation task. As a result, despeckling is a fundamental preprocessing step for applications using PolSAR data.

As reviewed in [1] and [2], various PolSAR filters have been proposed in the literatures, which can be generally categorized into following five classes: local filters; nonlocal means (NLM) based methods; partial differential equation based methods; variational methods; and machine learning based methods. One of the most classical local filters is the refined Lee filter [3], which was developed based on the linear minimum mean-squared error (LMMSE) estimator originally designed for single-polarization SAR despeckling [4]. Inspired by the refined Lee filter, a number of LMMSE-based PolSAR filtering algorithms have been developed [5], [6]. In the last few years, the NLM filter, which was originally designed for digital image denoising [7], has been a hot topic in PolSAR image despeckling [8]–[11]. The NLM filter not only searches and compares the values in a single point in a small local window but also the geometrical configuration in the whole image, thereby obtaining more robust results. In recent years, anisotropic diffusion based filters [12], [13], mean shift based filters [14], variational-based filters [15], [16], and the machine learning based filters [17], [18] have also been developed for PolSAR data despeckling.

The interest in PolSAR data has significantly increased in recent years, especially after the launch of spaceborne missions which can work in several different modes. Furthermore, some airborne missions, such as the NASA Jet Propulsion Laboratory (JPL) AIRSAR system, are now capable of acquiring multifrequency SAR signals. Compared with conventional monopolarized SAR, multifrequency fully PolSAR systems provide more information about a scene and have proved their advantages in many applications [19], [20]. When dealing with the despeckling problem of such data, a traditional way is to filter each band of the data independently by a certain single-frequency filter. Theoretically speaking, a filter that utilizes the multifrequency polarimetric information should be able to obtain better results. However, to the best of our knowledge, a filter specifically designed for multifrequency fully PolSAR data has not been presented in the literature to date.

In this paper, an iterative NLM filter is developed to tackle the issue of multifrequency PolSAR image despeckling. The main

innovations and differences of the proposed method compared with other PolSAR NLM filters are as follows: first, the proposed method is developed based on a space-frequency information joint covariance matrix (SF-JCM), which can exploit both the multifrequency polarimetric information and the correlation between any two pixels inside an image patch and obtain multiple estimations for each pixel, thus obtaining a more robust filtering performance; and second, by utilizing the multifrequency polarimetric information, a preselection step is employed to accelerate the filtering procedure and effectively retain the image details.

The rest of this paper is organized as follows. Section II describes the statistical model of single-frequency PolSAR data, and the idea of the multifrequency polarimetric information JCM is introduced. In Section III, the filtering framework of the proposed iterative multifrequency PolSAR NLM (IMP-NLM) method is presented. The idea of SF-JCM is also introduced and the benefits of employing SF-JCM are analyzed. Then, in Section IV, we describe the filtering experiments conducted on a simulated dataset and two real multifrequency PolSAR datasets acquired by the AIRSAR system. Finally, we draw our conclusions in Section V.

II. STATISTICAL MODEL OF POLSAR DATA AND THE MULTIFREQUENCY POLARIMETRIC INFORMATION JCM

A. Statistical Model of Single-Frequency PolSAR Data

A single-frequency fully polarimetric SAR system measures the complex scattering information of an observed target with quad-polarizations. In the monostatic and reciprocal backscattering case, the back-scattered radar signal from each cell of the PolSAR system can be characterized by the following target scattering vector:

$$k = (S_{\mathrm{HH}}, \sqrt{2}S_{\mathrm{HV}}, S_{\mathrm{VV}})^T \qquad (1)$$

where S_{HV} denotes the scattering component of the vertical transmitting and horizontal receiving polarizations, which is combined by the phase ϕ_{HV} and the amplitude $|S_{\mathrm{HV}}| : S_{\mathrm{HV}} = |S_{\mathrm{HV}}|e^{j\phi_{\mathrm{HV}}}$, where j denotes the imaginary part. Single-look polarimetric data can also be represented by polarimetric coherency matrix or covariance matrix. The polarimetric covariance matrix is the outer product of the associated target vector k with its conjugate transpose k^{H}

$$
\begin{aligned}
C &= kk^{\mathrm{H}} \\
&= \begin{bmatrix}
|S_{\mathrm{HH}}|^2 & \sqrt{2}S_{\mathrm{HH}}S_{\mathrm{HV}}^* & S_{\mathrm{HH}}S_{\mathrm{VV}}^* \\
\sqrt{2}S_{\mathrm{HV}}S_{\mathrm{HH}}^* & 2|S_{\mathrm{HV}}|^2 & \sqrt{2}S_{\mathrm{HV}}S_{\mathrm{VV}}^* \\
S_{\mathrm{VV}}S_{\mathrm{HH}}^* & \sqrt{2}S_{\mathrm{VV}}S_{\mathrm{HV}}^* & |S_{\mathrm{VV}}|^2
\end{bmatrix}.
\end{aligned} \qquad (2)
$$

In order to compress data and reduce speckle, PolSAR data are frequently multilook processed in the imaging process, by averaging several neighboring single-look pixels. This leads to

the multilook polarimetric covariance matrix

$$
\begin{aligned}
C_L &= \frac{1}{L}\sum_{i=1}^{L} k(i)k(i)^{\mathrm{H}} \\
&= \begin{bmatrix}
\langle |S_{\mathrm{HH}}|^2 \rangle & \langle \sqrt{2}S_{\mathrm{HH}}S_{\mathrm{HV}}^* \rangle & \langle S_{\mathrm{HH}}S_{\mathrm{VV}}^* \rangle \\
\langle \sqrt{2}S_{\mathrm{HV}}S_{\mathrm{HH}}^* \rangle & \langle 2|S_{\mathrm{HV}}|^2 \rangle & \langle \sqrt{2}S_{\mathrm{HV}}S_{\mathrm{VV}}^* \rangle \\
\langle S_{\mathrm{VV}}S_{\mathrm{HH}}^* \rangle & \langle \sqrt{2}S_{\mathrm{VV}}S_{\mathrm{HV}}^* \rangle & \langle |S_{\mathrm{VV}}|^2 \rangle
\end{bmatrix}.
\end{aligned} \qquad (3)
$$

To date, most of the PolSAR filters have been developed based on the assumption of "fully developed speckle" [21]. It is well known that, for fully developed speckle, the target vector can be modeled as having a multivariate complex Gaussian distribution, and the L-look covariance matrix C_L follows a complex Wishart distribution $Wc(q, L, Z)$ [22]:

$$P(C_L|Z) = \frac{L^{qL}|C_L|^{L-q}\exp\{-LTr(Z^{-1}C_L)\}}{Q(L,q)|Z|^L} \qquad (4)$$

with

$$Q(L,q) = \pi^{q(q-1)/2}\prod_{i=1}^{q}\Gamma(L-i+1) \qquad (5)$$

where Z is the population covariance matrix and $Tr(\cdot)$ denotes the trace operator. The parameter $q = 3$ is the dimension of the polarimetric covariance matrix.

B. Multifrequency Polarimetric Information JCM

1) For Single-Look Datasets: To obtain more robust filtering results for multifrequency PolSAR data, it is important to simultaneously take into account the polarimetric information from the data of all frequencies. Here, we introduce a joint scattering vector (JSV) for the PolSAR data with n bands, which is formulated as

$$v = [k_1^T k_2^T \cdots k_n^T]^T \qquad (6)$$

where k_n is the scattering vector of the data of band n, It can be easily concluded that, as the scattering vector of single-frequency data, this JSV can still be modeled by a multivariate complex Gaussian distribution. The associated single-look JCM is then derived as

$$
\begin{aligned}
J &= vv^{\mathrm{H}} \\
&= \begin{bmatrix}
A_{11} & A_{12} & \cdots & A_{1n} \\
A_{12} & A_{22} & \cdots & A_{2n} \\
\cdots & \cdots & \cdots & \cdots \\
A_{1n} & A_{2n} & \cdots & A_{nn}
\end{bmatrix}
\end{aligned} \qquad (7)
$$

where each element is $A_{ab} = k_ak_b^{\mathrm{H}}$. The dimension of the above JCM is $q = 3n$. As we can see, the matrices in the diagonal terms of the above JCM are the standard 3×3 single-look polarimetric covariance matrices of the data of each band. For the off-diagonal term A_{ab}, it is a complex matrix containing information about the polarimetric cross-correlation between band a and band b. The above JCM includes the polarimetric information from each frequency, as well as their cross-correlation.

2) For Multilook Datasets: For most of the current multi-frequency PolSAR systems, the multilook process for the data of each frequency in the imaging procedure is undertaken independently. The data of each band are then compressed and can only be represented by covariance or coherency matrices. Users cannot obtain the target vector data of a multilook image, and in such a case, the off-diagonal terms in (7) is unavailable. Therefore, for multifrequency multilook PolSAR data, the JCM reduces to

$$J_L = \begin{bmatrix} \langle A_{11} \rangle & 0_{3\times3} & \cdots & 0_{3\times3} \\ 0_{3\times3} & \langle A_{22} \rangle & \cdots & 0_{3\times3} \\ \cdots & \cdots & \cdots & \cdots \\ 0_{3\times3} & 0_{3\times3} & \cdots & \langle A_{nn} \rangle \end{bmatrix} \qquad (8)$$

where $0_{3\times3}$ represents a 3×3 all-zero matrix. Clearly, compared with the JCM for single-look data, J_L cannot exploit the polarimetric cross-correlation information between the data of any two different bands.

III. ITERATIVE MULTIFREQUENCY POLSAR NLM

Inspired by the iterative NLM filtering framework for single-polarization SAR data presented in [23], an iterative NLM method is proposed in this paper to process multifrequency PolSAR data. The main idea behind the proposed method is that, in each iteration, the polarimetric information from both the speckled image and the estimated image obtained in the last iteration is employed to refine the weight calculation of the sample pixels. A main innovation of the proposed method is that we take the space-frequency information JCM of a patch as the basic processing unit, rather than the covariance matrix of a single pixel. In the following two parts of this section, the concept of the space-frequency information JCM and the basic framework of IMP-NLM are described.

A. Space-Frequency Information JCM

Comparing the similarity between image patches is a vital step for the NLM-based methods, which is often accomplished by comparing each pair of pixels in the same position and taking their sum as the similarity of the two patches. Although this approach has its advantages, its drawbacks are also distinct. For example, for a point target with one or two pixels located in a large homogeneous area, if we compare the image patch centered on this target and other homogeneous patches by the traditional approach, the patches could be considered to be quite similar. As a result, this point target can be easily smeared after the weighted averaging. In such a case, taking into account the similarity or correlation between the pixels inside the patch is necessary.

In this paper, to alleviate the aforementioned drawback of the NLM filters, we introduce the concept of the space-frequency information JCM to represent the polarimetric information of each image patch. For a multifrequency single-look PolSAR image patch, by integrating the spatial correlation information into the multifrequency information JSV introduced in Section II,

we can get the following space-frequency information JSV:

$$s = [v_1^T v_2^T \cdots v_m^T]^T$$
$$= [k_{11}^T k_{12}^T \cdots k_{1n}^T k_{21}^T k_{22}^T \cdots k_{mn}^T]^T \qquad (9)$$

where m is the number of pixels in the patch. s is with the size of 3 mn $\times$ 1, containing the fully polarimetric scattering information of all pixels in a patch of all bands. The single-look SF-JCM for a patch is then constructed as

$$J = ss^H$$
$$= \begin{bmatrix} k_{11}k_{11}^H & k_{11}k_{12}^H & \cdots & k_{11}k_{1n}^H & \cdots & k_{11}k_{mn}^H \\ k_{12}k_{11}^H & k_{12}k_{12}^H & \cdots & k_{12}k_{12}^H & \cdots & k_{12}k_{mn}^H \\ \cdots & \cdots & \cdots & \cdots & \cdots & \cdots \\ k_{1n}k_{11}^H & \cdots & \cdots & k_{1n}k_{1n}^H & \cdots & k_{1n}k_{mn}^H \\ \cdots & \cdots & \cdots & \cdots & \cdots & \cdots \\ k_{mn}k_{11}^H & \cdots & \cdots & k_{mn}k_{1n}^H & \cdots & k_{mn}k_{mn}^H \end{bmatrix}$$
$$(10)$$

where k_{mn} denotes the target scattering vector of the mth pixel in the nth band. The dimension of the SF-JCM is $q = 3$ mn. Clearly, in the SF-JCM, the diagonal terms are the standard covariance matrices of the different pixels in the different bands, while the off-diagonal terms are complex matrices containing polarimetric cross-correlation information in both the spatial domain and frequency domain. Similarly, the SF-JCM for multilook data reduces to

$$J_L =$$
$$\begin{bmatrix} \langle k_{11}k_{11}^H \rangle & 0_{3\times3} & \cdots & \cdots & 0_{3\times3} & 0_{3\times3} \\ 0_{3\times3} & \langle k_{12}k_{12}^H \rangle & 0_{3\times3} & \cdots & \cdots & 0_{3\times3} \\ 0_{3\times3} & 0_{3\times3} & \cdots & 0_{3\times3} & \cdots & 0_{3\times3} \\ 0_{3\times3} & \cdots & 0_{3\times3} & \langle k_{1n}k_{1n}^H \rangle & 0_{3\times3} & 0_{3\times3} \\ 0_{3\times3} & \cdots & \cdots & 0_{3\times3} & \cdots & 0_{3\times3} \\ 0_{3\times3} & 0_{3\times3} & \cdots & \cdots & 0_{3\times3} & \langle k_{mn}k_{mn}^H \rangle \end{bmatrix}$$
$$(11)$$

The benefits of employing the SF-JCM are as follows:
1) *Employing more information hidden in the dataset:* The addition of the spatial and frequency dimensions to the data enlarges the considered data element model. In other words, the spatial and frequency dimensions are employed to improve the characterization of each scene location. Furthermore, by integrating the correlation information between two pixels in a patch, the aforementioned point target smearing problem can be effectively relieved.
2) *Multiple estimations:* The proposed method takes the SF-JCM of a patch as the basic unit. As a result, given a reference image patch and in the nonlocal weighted averaging step, the covariance matrices of all the pixels in this patch (the matrices of the diagonal terms in JCM) can be simultaneously processed. Hence, theoretically, we can obtain m estimations for each pixel in the image after filtering
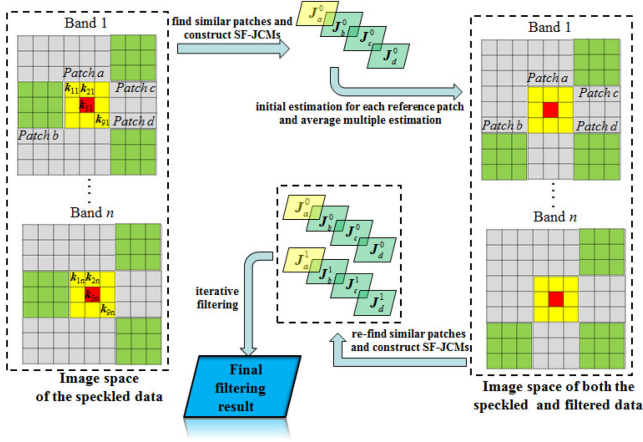
Fig. 1. Flowchart of the IMP-NLM method, where k denotes the scattering vector of a pixel and J_a^0 denotes the SF-JCM of the reference patch in the speckled image constructed by (9) and (10).

all the patches. By averaging these multiple estimations, the filtering result is much more robust.

B. Iterative Multifrequency PolSAR NLM

The basic idea of the proposed IMP-NLM method is shown in Fig. 1. In each iteration, the polarimetric information from both the speckled image and the estimated image obtained in the last iteration is employed to refine the weight calculation of the sample pixels. This iterative NLM process is formulated as

$$\hat{\boldsymbol{J}}_x^t = \sum_{y=1}^M w_{(x,y)}^t \boldsymbol{J}_y \bigg/ \sum_{y=1}^M w_{(x,y)}^t \qquad (12)$$

with the weight

$$w_{(x,y)}^t = \exp\left\{ -\left[\frac{D(\boldsymbol{J}_x^* = \boldsymbol{J}_y^* | \boldsymbol{J}_x, \boldsymbol{J}_y, \hat{\boldsymbol{J}}^{t-1})}{h} \right]^2 \right\} \qquad (13)$$

where $\boldsymbol{J}$, $\boldsymbol{J}^*$, and $\hat{\boldsymbol{J}}^{t-1}$ are the SF-JCMs of the speckled image, the noise-free image, and the image obtained in the last iteration, respectively; M denotes the size of the search window; and h is a normalization parameter. The numerators inside the weight kernel denote the similarity between two JCMs centered on pixel x and pixel y, given the speckled image and the previously estimated image.

From the aspect of probability statistics, the similarity measure in (13) can be rewritten as

$$D(\boldsymbol{J}_x^* = \boldsymbol{J}_y^* | \boldsymbol{J}_x, \boldsymbol{J}_y, \hat{\boldsymbol{J}}^{t-1}) = P(\boldsymbol{J}_x^* = \boldsymbol{J}_y^* | \boldsymbol{J}_x, \boldsymbol{J}_y, \hat{\boldsymbol{J}}^{t-1}). \qquad (14)$$

Under a Bayesian framework, in the absence of any information on $P(\boldsymbol{J}_x, \boldsymbol{J}_y)$, and assuming that the event $P(\boldsymbol{J}_x^* = \boldsymbol{J}_y^* | \boldsymbol{J}_x, \boldsymbol{J}_y)$ is independent of $\hat{\boldsymbol{J}}^{t-1}$, the following relation holds [23]:

$$P(\boldsymbol{J}_x^* = \boldsymbol{J}_y^* | \boldsymbol{J}_x, \boldsymbol{J}_y, \hat{\boldsymbol{J}}^{t-1}) = P(\boldsymbol{J}_x^* = \boldsymbol{J}_y^* | \boldsymbol{J}_x, \boldsymbol{J}_y)$$
$$P(\boldsymbol{J}_x^* = \boldsymbol{J}_y^* | \hat{\boldsymbol{J}}^{t-1}) \qquad (15)$$

Clearly, the first term of the right-hand side of (15) denotes the probability of having identical noise-free values, given the observed speckled image. In this paper, we deploy the Wishart likelihood-ratio test statistic [24] to calculate this term. Given two independent $q \times q$ Hermitian positive definite (HPD) SF-JCMs $\boldsymbol{J}_x$ and $\boldsymbol{J}_y$, which follow complex Wishart distributed, i.e., $\boldsymbol{J}_x \in Wc(q, L, \boldsymbol{J}_x^*)$ and $\boldsymbol{J}_y \in Wc(q, L, \boldsymbol{J}_y^*)$, we consider the null hypothesis, $\boldsymbol{J}_x^* = \boldsymbol{J}_y^*$, which states that the two SF-JCMs are equal, against the alternative hypothesis, $\boldsymbol{J}_x^* \neq \boldsymbol{J}_y^*$. If the hypothesis is true, the Wishart likelihood-ratio test statistic can be deduced as [24]

$$P(\boldsymbol{J}_x^* = \boldsymbol{J}_y^* | \boldsymbol{J}_x, \boldsymbol{J}_y) \propto 2q \ln 2 + \ln |\boldsymbol{J}_x| + \ln |\boldsymbol{J}_y|$$
$$- 2 \ln |\boldsymbol{J}_x + \boldsymbol{J}_y|. \qquad (16)$$

Several issues should be considered before applying (16): First, the Wishart likelihood-ratio test statistic involves the matrix logarithm, which means that the SF-JCMs have to be full rank ($|\boldsymbol{J}| \neq 0$). However, for the single-look SF-JCM, since the number of looks is much smaller with respect to the dimension of the matrix ($L \ll q$), numerical instability can happen in the filtering process. To avoid numerical problems, we employ a preprocessing step, as in [10], to transform the SF-JCM to ensure it is full rank. The transformed matrix T is denoted as

$$\forall s, \boldsymbol{T}_{s,s} = \boldsymbol{J}_{s,s}; \forall s \neq t, \boldsymbol{T}_{s,t} = L/q \cdot \boldsymbol{J}_{s,t} \qquad (17)$$

where s and t are the indices of the elements of the matrix. It was proved in [10] that the transformed data by (17) can still be modeled by the Wishart distribution defined in (4), and the likelihood-ratio test is still valid for the rescaled data. Note that this transformation step is only taken to calculate the weights, while the weighted averaging step is conducted using the original data. Second, for the multilook SF-JCM in (11), it is a block diagonal matrix. Although this matrix does not follow the complex Wishart distribution $Wc(q, L, \boldsymbol{Z})$, the likelihood-ratio test statistic in (16) is still valid. We refer the reader to [10] for proof of the above conclusion.

The covariance matrices lie on the symmetric cone of the HPD matrices, this is a Riemannian manifold. For the calculation of the second term of (15), we use the affine invariant metric proposed in [25] to deal with the HPD matrices, i.e.,

$$P(\boldsymbol{J}_x^* = \boldsymbol{J}_y^* | \hat{\boldsymbol{J}}^{t-1}) \propto || \log \mathrm{m}(\hat{\boldsymbol{J}}_x^{t-1}) - \log \mathrm{m}(\hat{\boldsymbol{J}}_y^{t-1}) ||_F \quad (18)$$

where $\log \mathrm{m}(\cdot)$ denotes the matrix logarithm and $|| \cdot ||_F$ is the Frobenius norm.

C. Preselection Step

In practice, the relatively high computational load hampers the applicability of NLM filters. Furthermore, the iterative strategy deployed in the proposed method exerts even more computational burden. In this paper, we employ a fast preselection step

TABLE I
SIGMA RANGE η_1 AND η_2 FOR DIFFERENT SIGMA
VALUES ξ AND DIFFERENT NUMBERS OF LOOKS

		η_1	η_2
1-look intensity	$\xi = 0.7$	0.254	2.582
	$\xi = 0.8$	0.168	3.094
	$\xi = 0.9$	0.084	3.941
4-look intensity	$\xi = 0.7$	0.560	1.627
	$\xi = 0.8$	0.480	1.804
	$\xi = 0.9$	0.378	2.094

to select similar sample pixels in the search window to accelerate the filtering procedure. Furthermore, discarding dissimilar sample pixels can prevent some image details from smearing.

The preselection step taken in this paper is inspired by the sigma filter [26]–[28]. The idea of the sigma filter provides a way to quickly select similar pixels in the SAR images. Given a sigma value ξ and the *a priori* mean $\tilde{x}$ of the intensity of the target pixel, pixels within the range $(\eta_1 \tilde{x}, \eta_2 \tilde{x})$ are considered as similar pixels with respect to the target one. Let $I_1 = \eta_1 \tilde{x}$ and $I_2 = \eta_2 \tilde{x}$, to calculate the η values, the following condition should be satisfied:

$$\xi = \int_{I_1}^{I_2} p_L(I) dI \tag{19}$$

where $p_L(I)$ denotes the probability distribution of the intensity I, given the number of looks L; besides, to maintain the mean value of the intensity $\bar{I}$, the following condition should be also considered:

$$\bar{I} = \frac{1}{\xi} \int_{I_1}^{I_2} I p_L(I) dI. \tag{20}$$

We refer the readers to [27] for more details about the above derivations and the way to solve (19) and (20).

The sigma range η_1 and η_2 for different sigma values ξ and different numbers of looks are listed in Table I. In this paper, to taken into account more polarimetric information, the intensity information of all the polarizations and all the frequencies is used for the preselection. Only pixels selected by all the polarizations and all the frequencies are included in the filtering. In addition, in each iteration, we take the filtering result of each intensity image in the last iteration as the *a priori* mean value to select similar pixels.

D. Choice of Filtering Parameters

There are three main filtering parameters that need to be determined when applying the proposed method, which are, respectively, parameter h in the weight kernel, sigma value ξ, and the iteration times t.

In this paper, h is automatically determined by the "noise estimator" proposed in [29]: before each iteration step, a histogram of the absolute values of the similarity between any two neighboring SF-JCMs along a certain direction throughout the image is computed as (15), and h is set to be equal to the 80% value of its integral. By doing so, h can be adaptively set as a

larger value to better reduce the speckle, if the speckle level of the image is high, and vice versa. In practice, h can be fine-tuned to obtain better results.

For the sigma value ξ, through a number of experiments, we found that it is better to set as 0.9 or 0.8 for four-look images, and set as 0.8 or 0.7 for single-look images. Furthermore, we found that, in most cases, the filtering results with two iterations are good enough when processing four-look images, while three iterations are enough for single-look images.

IV. EXPERIMENTAL PART

In the experimental part, to illustrate the filtering performance of the proposed IMP-NLM method, the results obtained with a simulated dataset and two real multifrequency PolSAR datasets acquired by the AIRSAR system are reported. Three typical and state-of-the-art PolSAR filters were implemented for comparison purposes: the pretest NLM filter [7], the PolSAR simultaneous sparse coding (SSC) filter [16], and the PolSAR nonlocal total variation (NLTV) filter [15]. For each method, the size of the searching window is fixed as 15×15 to make a compromise between reducing speckle and retaining details, and the patch window size is set as 3×3 to ease the computational load and better preserve point targets. For reproducibility, the test dataset and the source codes of the proposed method and the quantitative indicators which were coded in MATLAB, can be downloaded from the link (http://sendimage.whu.edu.cn/en/resources/).

A. Experiments With Simulated Multifrequency PolSAR Data

For the simulation method proposed in [21], the key to simulating a PolSAR image with any number of looks is to simulate single-look data, and then average several simulations to form multilook data. To simulate single-look data, we must generate the target scattering vector. Based on the above analysis, we employed the following procedure to simulate a multifrequency PolSAR dataset with N different classes of land-objects:

1) Given a real AIRSAR dataset with P, L, and C bands, select several homogeneous areas for each land-object class in each band and calculate the mean covariance matrices $C_{1C}, C_{2C}...C_{1P}, C_{2P}...C_{Np}$.
2) For each mean covariance matrix C (the real covariance matrix of each class in the different bands), compute $C^{1/2}$, satisfying

$$C^{1/2}(C^{1/2})^{\mathrm{H}} = C. \tag{21}$$

3) Simulate a complex random vector α that follows a complex normally distribution with zero mean. This process can be accomplished by independently constructing the real and imaginary parts of each element of α, which all follows a normal distribution with zero mean and 0.5 variance.
4) The target scattering vector k is then given by

$$k = C^{1/2}\alpha. \tag{22}$$

We simulated a single-look PolSAR dataset with P, L, and C bands, as shown in Fig. 2. To quantitatively evaluate the filtering performances of the different methods on the simulated dataset,
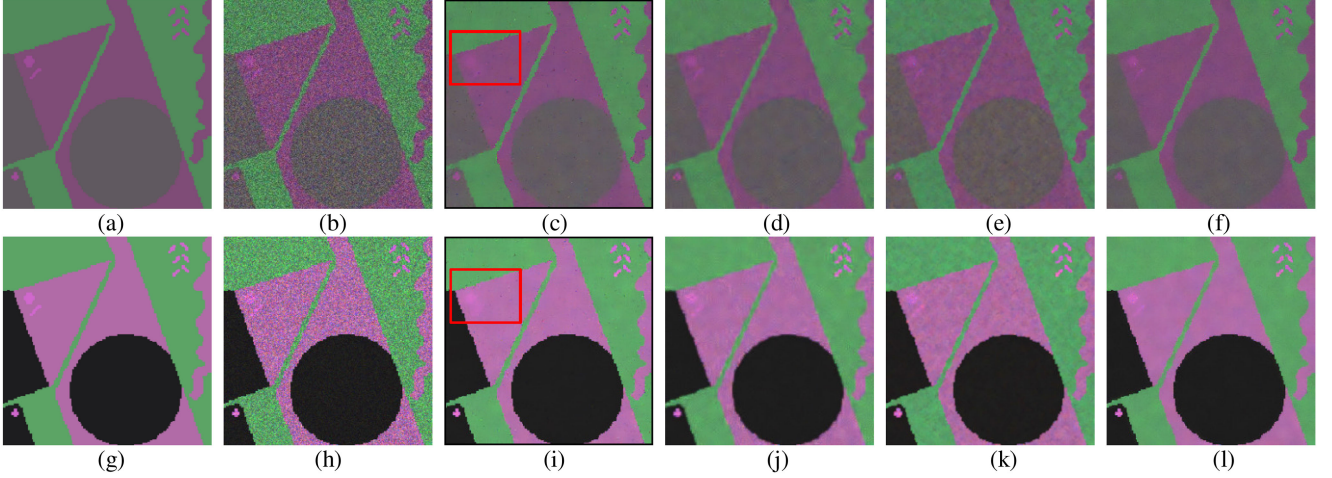
Fig. 2. (a)–(f) P-band Pauli RGB images of the simulated data, the single-look speckled data, the pretest NLM filtered data, the PolSAR SSC filtered data, the PolSAR NLTV filtered data, and the IMP-NLM filtered data, respectively. (g)–(l) Three-band composite RGB images (R: C-band intensity; G: L-band intensity; B: P-band intensity) of the corresponding data.

the equivalent number of looks (ENL), the edge reconstruction error (ERR$_{\text{edge}}$) [25], the mean of ratio (MOR), and the absolute relative bias (ARB) [2] are employed.

ENL: The ENL is an important indicator to assess the amount of speckle in SAR images, and is generally computed as

$$\text{ENL} = 1/\sigma_v^2 \tag{23}$$

where σ_v denotes the coefficient of variation of the intensity in homogeneous areas.

ERR$_{\text{edge}}$: The ERR$_{\text{edge}}$ is an indicator with reference, given by

$$\text{ERR}_{\text{edge}} = \left[\frac{\sum_{i=1}^{N} f(i) \|\mathbf{C}_d(i) - \mathbf{C}_r(i)\|_F^2}{9 \cdot \sum_{i=1}^{N} f(i)} \right]^{\frac{1}{2}} \tag{24}$$

where N is the total pixel number of the image; $\mathbf{C}_d$ and $\mathbf{C}_r$ denote the covariance matrices of the despeckled image and the clean image, respectively; and $\| \cdot \|_F$ is the Frobenius norm. $f(i)$ is set as 1, if pixel i locates on the edge; otherwise, it is set as 0. A lower ERR$_{\text{edge}}$ index value indicates a better edge-preservation result.

MOR: Theoretically, an ideal SAR filter can well maintain the mean intensity value of the homogeneous areas in the image and the ratio image between the speckled intensity image and the filtered intensity image should be pure random noise. Therefore, the corresponding MOR value of a good filter that can effectively preserve the radiometric information should be very close to 1.

ARB: For image interpretation tasks, maintaining the polarimetric scattering mechanisms of PolSAR data is important when applying a filter. The ARB is an index often used to assess the scattering mechanism preservation capability of a filter. For every scattering class a in a simulated PolSAR data, the ARB of the estimated value $\hat{\theta}$ for any given parameter θ is calculated as

$$\text{ARB}_{\theta, a} = \left| \frac{\theta_a - \hat{\theta}_a}{\theta_a} \right|. \tag{25}$$

TABLE II
QUANTITATIVE ASSESSMENT RESULTS FOR THE SIMULATED DATASET FILTERED BY THE DIFFERENT METHODS

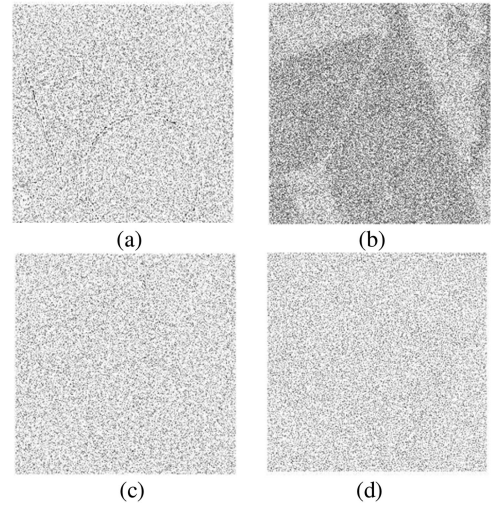|	ENL	ERR$_{\text{edge}}$	MOR	ARB$_H$	ARB$_A$	ARB$_{\bar{\alpha}}$
Pretest NLM	75.6	0.0405	0.994	0.010	0.036	0.023
PolSAR SSC	71.0	0.0446	0.961	0.029	0.140	0.032
PolSAR NLTV	59.8	0.0421	0.972	0.033	0.116	0.030
IMP-NLM	77.7	0.0395	0.988	0.011	0.031	0.024

Fig. 3. P-band ratio images for (a) the pretest NLM filter, (b) the PolSAR SSC filter, (c) the PolSAR NLTV filter, and (d) the proposed IMP-NLM method.

Then, a median operator across all the bands of the data and the various scattering classes is conducted. In this paper, we use the Cloude polarimetric decomposition parameters (entropy H, anisotropy A, and average alpha angle $\bar{\alpha}$) [31] to assess the ability of the filters in preserving the polarimetric information as suggested in [2], since they can directly reflect the physical nature of the scattering mechanism within the resolution cell.
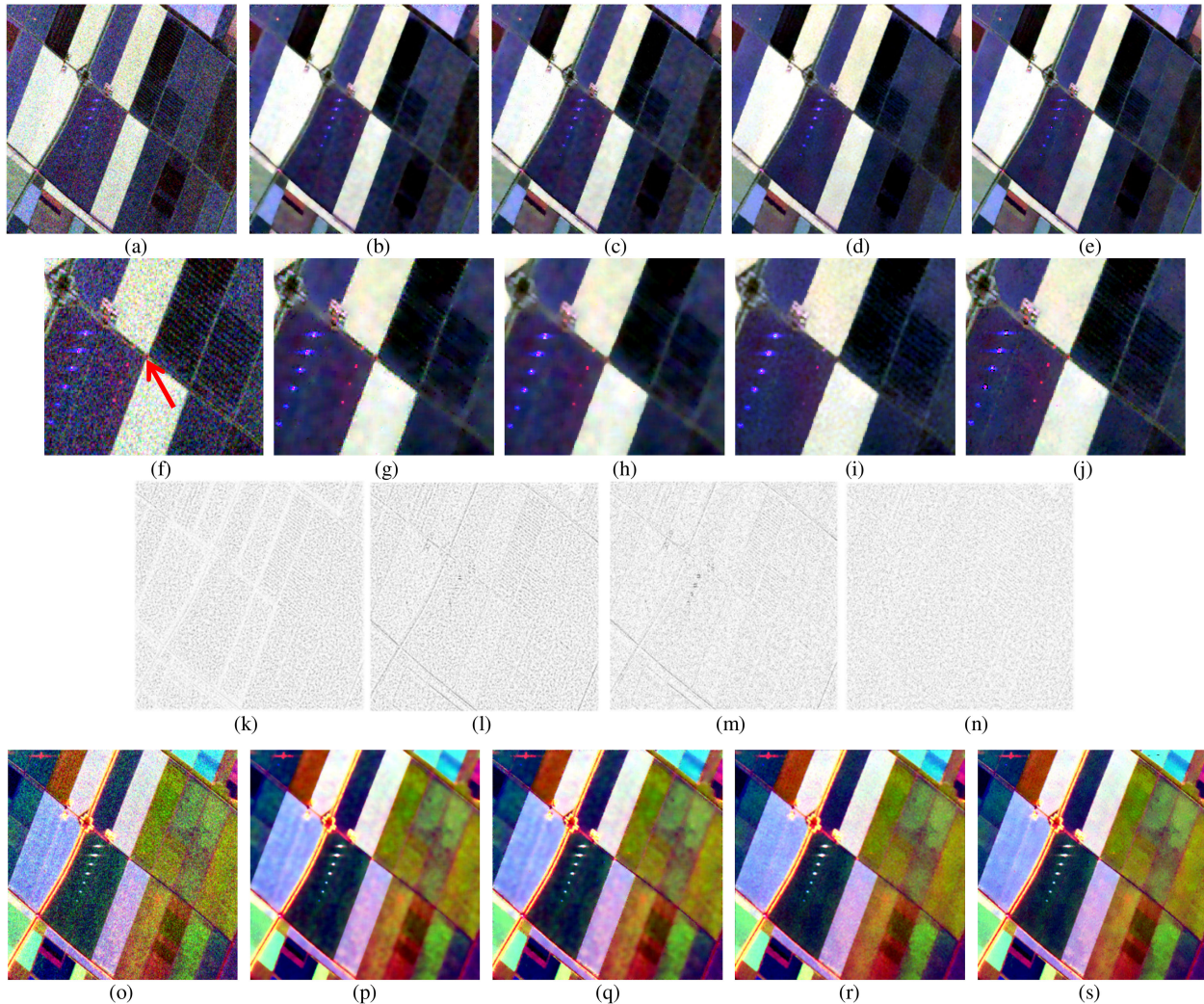
Fig. 4.   (a)–(e) C-band images of the speckled data, the pretest NLM filtered data, the PolSAR SSC filtered data, the PolSAR NLTV filtered data, and the IMP-NLM filtered data, respectively. (f)–(j) Subimages cropped from (a)–(e), respectively. (k)–(n) Ratio images of the different filters. (o)–(s) Three-band composite RGB images (R: C-band intensity; G: L-band intensity; B: P-band intensity) of the corresponding data.

In this paper, we calculate the indicators in the images with the different bands, and take the mean values to assess the filters. The quantitative assessment results of the different filtering methods are listed in Table II. As can be observed in Fig. 2, at first sight, the pretest NLM filter shows a positive filtering result: the speckle is notably reduced and the edges are well preserved. However, one can also observe that some strong noise still resides in the image and some details are badly blurred (marked by the red rectangles). Compared with the pretest NLM filter, the PolSAR SSC filter better preserves the image details. However, some slight artifacts can be observed in the filtered image, which degrade the resolution of the image and cause its relatively high ERR_{edge} value. Clearly, among the four filters, the PolSAR NLTV method shows the worst performance in suppressing speckle. In fact, the studies in [1] and [15] also revealed that the PolSAR NLTV method often cannot effectively reduce the speckle when the level of speckle is high. As can be seen, the IMP-NLM filter obtains the best balance between reducing speckle and retaining image details, from both a visual inspec-

TABLE III
QUANTITATIVE ASSESSMENT RESULTS FOR THE REAL POLSAR
DATASETS FILTERED BY THE DIFFERENT METHODS

	Flevoland dataset			Kyoto dataset		
	ENL	EPD-ROA	MOR	ENL	EPD-ROA	MOR
Pretest NLM	63.3	0.811	1.006	80.4	0.753	0.972
PolSAR SSC	65.6	0.798	1.047	72.9	0.785	0.952
PolSAR NLTV	57.2	0.844	1.005	54.5	0.830	0.958
IMP-NLM	58.0	0.899	0.998	56.3	0.861	0.980

tion and the quantitative assessment. Besides, from the ARB values listed in Table II, we can see that the pretest NLM filter and the proposed filter have shown comparable performances in preserving the polarimetric information, while other two filters perform worse.

In Fig. 3, to further demonstrate the capability of the different filtering methods in retaining image details, we display the ratio images of the P band between the noisy intensity image and the
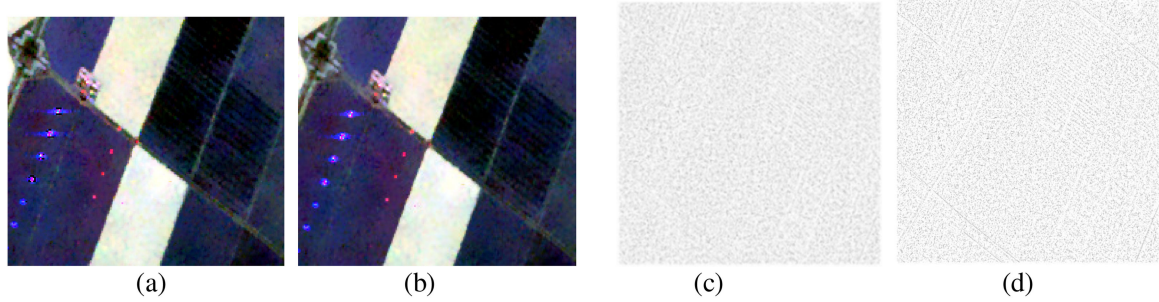
Fig. 5. (a) and (b) Subimages filtered by the IMP-NLM method with and without using the SF-JCM, respectively. (c) and (d) Ratio images of the IMP-NLM method with and without using the SF-JCM, respectively.
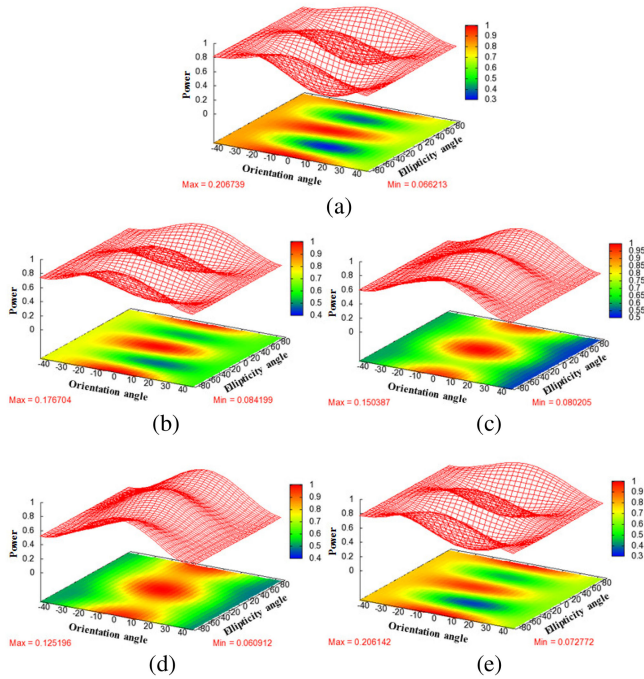

Fig. 6. C-band co-polarization signatures of a point target in the different images. (a) Original signature of the target. (b)–(e) Signature of the target in the images filtered by the pretest NLM filter, the PolSAR SSC method, the PolSAR NLTV method, and the IMP-NLM method, respectively.

filtered intensity images. Theoretically, for a very good SAR filter, the ratio image should be pure random noise. It can be observed that the ratio image for the IMP-NLM method has the appearance of random noise, while the edges are notably retained in the ratio image for the PolSAR SSC filter, which is consistent with the conclusions one can draw from the ERR_{edge} values.

B. Experiments With Two Real PolSAR Datasets

Two real PolSAR datasets were also used to validate the effectiveness of the proposed despeckling method. Both datasets were acquired by the AIRSAR system of NASA JPL. The AIRSAR system can simultaneously operate in fully polarimetric modes in the P (0.45 GHz), L (1.26 GHz), and C (5.31 GHz) bands. The AIRSAR project serves as a NASA radar technology test bed for demonstrating new radar technology. AIRSAR first flew in 1987 and continues to conduct at least one flight cam-

paign each year, either in the United States or on international missions [21].

Since the ERR_{edge} indicator must be calculated using a reference map which is infeasible for real dataset, we use the edge-preservation degree based on the ratio of average (EPD-ROA) [30] to replace it in this part. The EPD-ROA indicator is given by

$$\text{EPD} - \text{ROA} = \sum_{i=1}^{N} |\hat{I}_1(i)/\hat{I}_2(i)| \Big/ \sum_{i=1}^{N} |I_1(i)/I_2(i)| \quad (26)$$

where $\hat{I}_1$ and $\hat{I}_2$ denote the neighboring pixel values of the filtered image along a certain direction, respectively. Similarly, I_1 and I_2 denote the corresponding neighboring pixel values of the observed image. The closer an EPD-ROA value to 1, the better a filter maintains the edges. We calculate the EPD-ROA values of each filter along the vertical and horizontal directions, respectively, and take the mean value to assess the edge preservation capability.

1) Experiments With the Flevoland Dataset: The first real PolSAR dataset used for the comparison was acquired in Flevoland, the Netherlands, with P, L, and C bands. The filtering results of the different methods are shown in Fig. 4. The pretest NLM filter again shows a positive filtering performance, although a slight oversmoothing problem can be observed. The oversmoothing problem is more notable in the PolSAR SSC filtered image. Compared with the PolSAR SSC method, PolSAR NLTV shows a better result in retaining edges, as revealed by the EPD-ROA values in Table III and the ratio image. However, it can be clearly observed that some point targets are badly smeared by the PolSAR NLTV method. The superiority of the proposed IMP-NLM method in preserving edges, point targets, and radiometric information is evident, which is supported by the EPD-ROA and MOR values and the appearance of the ratio image.

The proposed IMP-NLM method is developed based on the SF-JCM, which can exploit both the multifrequency polarimetric information and the correlation between any two pixels inside an image patch. In Fig. 5, to demonstrate the benefits of using the SF-JCM, we display the filtering result of the IMP-NLM method without using the SF-JCM (in other word, comparing the similarity of two patches as the way of the traditional NLM methods and without considering multifrequency information). As we can see from Fig. 5(a) and (b), compared with the proposed IMP-NLM technique, the IMP-NLM method without using the
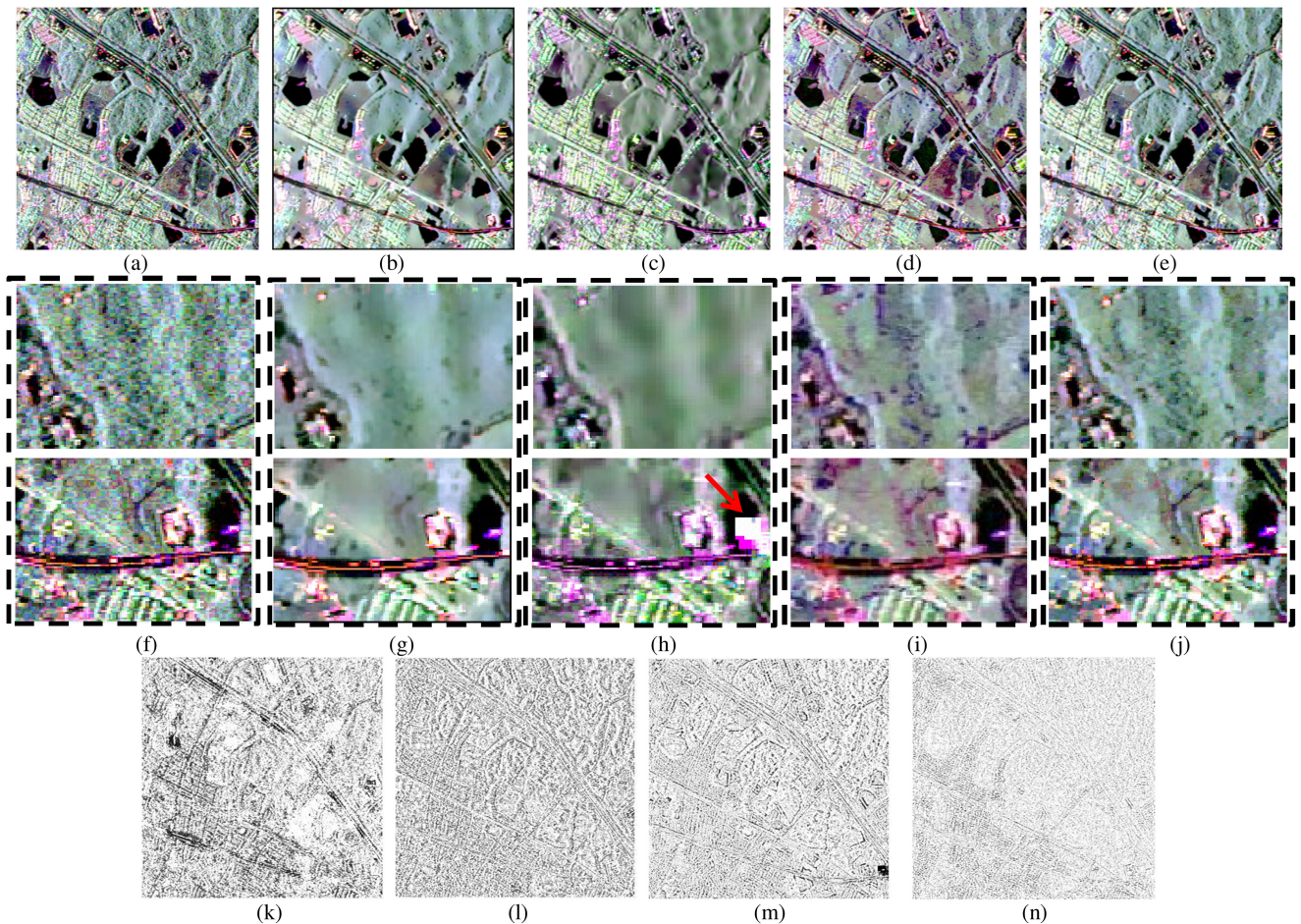
Fig. 7. Filtering results for the four-look Kyoto image. (a)–(e) C-band Pauli RGB images of the speckled data, the pretest NLM filtered data, the PolSAR SSC filtered data, the PolSAR NLTV filtered data, and the IMP-NLM filtered data, respectively. (f)–(j) Subimages cropped from (a)–(e), respectively. (k)–(n) Ratio images of the different filters.

SF-JCM smears the image details to a larger degree, especially for the point targets. The corresponding ratio images also support the above conclusion. Therefore, we can conclude that the outstanding filtering performance of the proposed method does benefit from the using of the SF-JCM.

Maintaining the signatures of the strong point targets is important when designing PolSAR filters. Unlike the scattering from distributed media, the returns from these targets come mainly from a few strong scatterers within a resolution cell, and it is better to maintain their original polarimetric information. To validate the capability of the despeckling methods in maintaining the polarimetric traits of point targets, we chose a target, as marked in Fig. 4(f), and plotted its C-band co-polarization signature for each filtered image (see Fig. 6). The polarimetric signatures [32] can visualize the normalized co-polarization or cross-polarization backscattered power of a target, given any orientation angle and any ellipticity angle. Clearly, distinct disagreements arise between the signatures from the original pixel and the pixels processed by the PolSAR SSC filter and the PolSAR NLTV filter, while much closer agreements are reached for the target processed by the IMP-NLM method.

2) Experiments With the Kyoto Dataset: The other dataset used to validate the effectiveness of the proposed method was acquired in Kyoto, Japan, with L and C bands. In Fig. 7, we display the filtering results of the C-band data. Compared with the simulated data and the real single-look data, the scene of this image is much more complicated, with lakes dominated by the surface scattering mechanism, forest areas dominated by the volume scattering mechanism, and urban areas with complicated scattering mechanisms. For this complicated image, the superiority of the proposed method is clearly evident. The oversmoothing problem in the pretest NLM filtered image is notable, and directly leads to the loss of many image details. From a visual inspection, both the PolSAR SSC filter and the NLTV filter appear to have changed the color of the image, indicating distortion of the polarimetric information to some degree, which can also be seen in the MOR values listed in Table III. For the PolSAR SSC filter, the oversmoothing problem in the forest areas is much more notable than that in the urban areas. Furthermore, some artifacts can be found in the PolSAR SSC filtered image, especially for some strong returns in the urban areas (marked by the red arrow in Fig. 7(h)). Clearly, the proposed IMP-NLM method shows very good results in preserving the scattering mechanisms and the spatial resolution of the images, as demonstrated by the quantitative indicators and the ratio image.

V. Conclusion

Multifrequency fully PolSAR systems provide more information about a scene. A common way of filtering multifrequency PolSAR data is to filter each band of the data independently, which does not take into account the polarimetric information from the data of all frequencies. In this paper, we have innovatively proposed a multifrequency fully PolSAR image despeckling method based on an iterative NLM filter. Compared with most of the traditional PolSAR NLM filters, the main innovations of the proposed method are as follows: first, the space-frequency information JCM is constructed as the basic processing unit, which can exploit both the multifrequency polarimetric information and the correlation between any two pixels inside the image patch to obtain multiple estimations for each pixel, thus obtaining a more robust filtering performance; and second, a preselection step is employed based on the idea of the sigma filter, utilizing the multifrequency polarimetric information, aiming at accelerating the filtering procedure and better retaining image details. Experiments on a simulated dataset and two real AIRSAR multifrequency datasets confirmed the outstanding filtering performance of the proposed method, especially in maintaining the polarimetric scattering information and the details of the images.

However, it should be pointed out that, although the sigma preselection step can ease the computational burden to some degree, the processing speed of the proposed filter is still relatively slow, mainly due to the iterative filtering framework and the high dimension of the SF-JCM which increases the burden of matrix operation. In the future, we will study more efficient strategy to fast discard dissimilar pixels to accelerate the filtering procedure.

References

[1] X. Ma, P. Wu, Y. Wu, and H. Shen, "A review on recent developments in fully polarimetric SAR image despeckling," *IEEE J. Sel. Topics Appl. Earth Observ. Remote Sens.*, vol. 11, no. 3, pp. 743–758, Mar. 2018.

[2] S. Foucher and C. López-Martínez, "Analysis, evaluation, and comparison of polarimetric SAR speckle filtering techniques," *IEEE Trans. Image Process.*, vol. 23, no. 4, pp. 1751–1764, Apr. 2014.

[3] J. S. Lee, M. R. Grunes, and G. D. Grandi, "Polarimetric SAR speckle filtering and its implication for classification," *IEEE Trans. Geosci. Remote Sens.*, vol. 37, no. 5, pp. 2363–2373, Sep. 1999.

[4] J. S. Lee, "Digital image enhancement and noise filtering by use of local statistics," *IEEE Trans. Pattern Anal. Mach. Intell.*, vol. PAMI-2, no. 2, pp. 165–168, Mar. 1980.

[5] J. S. Lee, M. R. Grunes, D. L. Schuler, E. Pottier, and L. F. Famil, "Scattering-model-based speckle filtering of polarimetric SAR data," *IEEE Trans. Geosci. Remote Sens.*, vol. 44, no. 1, pp. 176–187, Jan. 2006.

[6] G. Vasile, E. Trouve, J. S. Lee, and V. Buzuloiu, "Intensity-driven adaptive-neighborhood technique for polarimetric and interferometric SAR parameters estimation," *IEEE Trans. Geosci. Remote Sens.*, vol. 44, no. 6, pp. 1609–1621, Jun. 2006.

[7] A. Buades, B. Coll, and J. M. Morel, "A non-local algorithm for image denoising," in *Proc. IEEE Comput. Soc. Conf. Comput. Vis. Pattern Recognit.*, 2005, pp. 60–65.

[8] J. Chen, Y. Chen, W. An, Y. Cui, and J. Yang, "Nonlocal filtering for polarimetric SAR data: A pretest approach," *IEEE Trans. Geosci. Remote Sens.*, vol. 49, no. 5, pp. 1744–1754, May 2011.

[9] X. Xing, Q. Chen, S. Yang, and X. Liu, "An adaptive nonlocal mean filter for PolSAR data with shape-adaptive patches matching," *Sensors*, vol. 18, no. 7, 2018, Art. no. 2215.

[10] T. Yan, W. Yang, X. Yang, C. López-Martínez, H. Li, and M. Liao, "Polarimetric SAR despeckling by integrating stochastic sampling and contextual patch dissimilarity exploration," *IEEE J. Sel. Topics Appl. Earth Observ. Remote Sens.*, vol. 10, no. 6, pp. 2738–2753, Jun. 2017.

[11] C. A. Deledalle, L. Denis, F. Tupin, A. Reigber, and M. Jager, "NL-SAR: A unified non-local framework for resolution-preserving (Pol)(In)SAR denoising," *IEEE Trans. Geosci. Remote Sens.*, vol. 53, no. 4, pp. 2021–2038, Apr. 2015.

[12] X. Ma, H. Shen, L. Zhang, J. Yang, and H. Zhang, "Adaptive anisotropic diffusion method for polarimetric SAR speckle filtering," *IEEE J. Sel. Topics Appl. Earth Observ. Remote Sens.*, vo. 8, no. 3, pp. 1041–1050, Mar. 2015.

[13] X. Ma, H. Shen, and L. Zhang, "PolSAR anisotropic diffusion filter with a refined similarity measure and an adaptive fidelity constraint," *Int. J. Remote Sens.*, vol. 37, no. 24, pp. 5988–6011, 2016.

[14] F. Lang, J. Yang, D. Li, L. Shi, and J. Wei, "Mean-shift-based speckle filtering of polarimetric SAR data," *IEEE Trans. Geosci. Remote Sens.*, vol. 52, no. 7, pp. 4440–4454, Jul. 2014.

[15] X. Nie, H. Qiao, B. Zhang, and X. Huang, "A nonlocal TV-based variational method for PolSAR data speckle reduction," *IEEE Trans. Image Process.*, vol. 25, no. 6, pp. 2620–2634, Jun. 2016.

[16] X. Ma, H. Shen, X. Zhao, and L. Zhang, "SAR Image despeckling by the use of variational methods with adaptive nonlocal functionals," *IEEE Trans. Geosci. Remote Sens.*, vol. 54, no. 6, pp. 3421–3434, Jun. 2016.

[17] B. Xu, Y. Cui, B. Zuo, J. Yang, and J. Song, "Polarimetric SAR image filtering based on patch ordering and simultaneous sparse coding," *IEEE Trans. Image Process.*, vol. 54, no. 7, pp. 4079–4093, Jul. 2016.

[18] L. Gomez, L. Alvarez, L. Mazorra, and A. C. Frery, "Fully PolSAR image classification using machine learning techniques and reaction-diffusion systems," *Neurocomputing*, vol. 255, no. 13, pp. 52–60, 2017.

[19] J. Shi and J. Dozier, "On estimation of snow water equivalence using Sir-C/X-SAR," in *Proc. 2nd Int. Workshop Retrieval Bio- Geo-Phys. Parameters SAR Data Land Appl.*, Noordwijk, The Netherlands, 1998, pp. 503–510.

[20] L. F. Famil, E. Pottier, and J. S. Lee, "Unsupervised classification of multifrequency and fully polarimetric SAR images based on the H/A/alpha-Wishart classifier," *IEEE Trans. Geosci. Remote Sens.*, vol. 39, no. 11, pp. 2332–2342, Nov. 2001.

[21] J. S. Lee and E. Pottier, *Polarimetric Radar Imaging: From Basics to Applications*. Boca Raton, FL, USA: CRC Press, 2009.

[22] N. Goodman, "Statistical analysis based on a certain multivariate complex Gaussian distribution (an introduction)," *Ann. Math. Stat.*, vol. 34, no. 1, pp. 152–177, 1963.

[23] C. A. Deledalle, L. Denis, and F. Tupin, "Iterative weighted maximum likelihood denoising with probabilistic patch-based weights," *IEEE Trans. Image Process.*, vo. l8, no. 12, pp. 2661–2672, Dec. 2009.

[24] K. Conradsen, A. A. Nielsen, J. Schou, and H. Skriver, "A test statistic in the complex Wishart distribution and its application to change detection in polarimetric SAR data," *IEEE Trans. Geosci. Remote Sens.*, vol. 41, no. 1, pp. 4–19, Jan. 2003.

[25] O. D'Hondt, S. Guillaso, and O. Hellwich, "Iterative bilateral filtering of polarimetric SAR data," *IEEE J. Sel. Top. Appl. Earth Observ. Remote Sens.*, vol. 6, no. 3, pp. 1628–1639, Jun. 2013.

[26] J. S. Lee, "A simple speckle smoothing algorithm for synthetic aperture radar images," *IEEE Trans. Syst., Man, Cybern.*, vol. SMC-13, no. 1, pp. 85–89, Jan./Feb. 1983.

[27] J. S. Lee, J. H. wen, T. L. Ainsworth, K. S. Chen, and A. J. Chen, "Improved sigma filter for speckle filtering of SAR imagery," *IEEE Trans. Geosci. Remote Sens.*, vol. 47, no. 1, pp. 202–213, Jan. 2009.

[28] J. S. Lee, T. L. Ainsworth, Y. Wang, and K. S. Chen, "Polarimetric SAR speckle filtering and the extended sigma filter," *IEEE Trans. Geosci. Remote Sens.*, vol. 53, no. 3, pp. 1150–1160, Mar. 2015.

[29] J. Canny, "A computational approach to edge detection," *IEEE Trans. Pattern Anal. Mach. Intell.*, vol. PAMI-8, no. 6, pp. 679–698, Nov. 1986.

[30] H. Feng, B. Hou, and M. Gong, "SAR image despeckling based on local homogeneous region segmentation by using pixel-relativity measurement," *IEEE Trans. Geosci. Remote Sens.*, vol. 49, no. 7, pp. 2724–2737, Jul. 2011.

[31] S. R. Cloude and E. Pottier, "An entropy based classification scheme for land applications of polarimetric SAR," *IEEE Trans. Geosci. Remote Sens.*, vol. 35, no. 1, pp. 68–78, Jan. 1997.

[32] J. J. Zyl, H. A. Zebker, and C. Elachi, "Imaging radar polarization signatures: Theory and observation," *Radio Sci.*, vol. 22, pp. 529–543, 1987.

Xiaoshuang Ma received the B.S. degree in geographic information system from Hubei University, Wuhan, China, in 2011, and the Ph.D. degree in cartography and geographic Information engineering from Wuhan University, Wuhan, China, in 2016.

He is currently a Lecturer with the Department of Resources and Environmental Engineering, Anhui University, Hefei, China. His research interests include SAR image processing and interpretation.
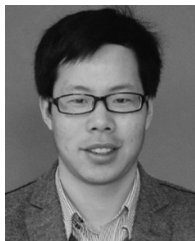
Penghai Wu (M'16) received the B.S. degree in environmental science from Anqing Normal College, Anqing, China, in 2009, and the M.S. degree in surveying and mapping engineering and the Ph.D. degree in cartography and geographical information engineering from Wuhan University, Wuhan, China, in 2011 and 2014, respectively.

He is currently an Associated Professor with the School of Resources and Environmental Engineering, Anhui University, Hefei, China. He has authored/co-authored more than 20 research papers that are published in journals such as *Remote Sensing of Environment* and IEEE TRANSACTIONS ON GEOSCIENCE AND REMOTE SENSING. His research interests include spatiotemporal fusion, the disaggregation of land surface temperature, the reconstruction of land surface temperature, and regional ecoenvironmental change.
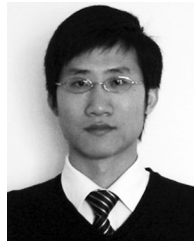
Huanfeng Shen (M'10–SM'13) received the B.S. degree in surveying and mapping engineering and the Ph.D. degree in photogrammetry and remote sensing from Wuhan University, Wuhan, China, in 2002 and 2007, respectively.

In 2007, he joined the School of Resource and Environmental Sciences, Wuhan University, where he is currently a Luojia Distinguished Professor. He has authored more than 100 research papers. His research interests include image-quality improvement, remote-sensing mapping and application, data fusion and assimilation, and regional and global environmental change.

Dr. Shen has been supported by several talent programs such as the Youth Talent Support Program of China (2015), China National Science Fund for Excellent Young Scholars (2014), and the New Century Excellent Talents by the Ministry of Education of China (2011). He is currently a Member of the Editorial Board of the *Journal of Applied Remote Sensing*.